

Structure Design and Electrifying Strategy of the High-torque Flux-switching Permanent-magnet Spherical Motor

Xiwen Guo^{1,2,4}, Zhibo Liu^{1,2}, Zhaowei Fang^{1,2}, Rui Zhou^{1,2}, Qunjing Wang^{1,2,3}, Ronglin Zhang⁵

¹ School of Electrical Engineering and Automation, Anhui University, Hefei, Anhui, China

² National Engineering Laboratory of Energy-saving Motor & Control Technique, Anhui University, Anhui, China

³ Industrial Power Saving and Safety Laboratory, Anhui University, Hefei, Anhui, China

⁴ Collaborative Innovation Centre of Industrial Energy-Saving and Power Quality Control, Anhui University, China

⁵ State Grid Lu'an Electric Power Supply Company, Lu'an, Anhui, China

E-mail: lzbahu@163.com

Abstract. To solve the problems of a no-core structure in the stator coil of the permanent-magnet spherical motor (PMSM), low-effective output torque and low-power density, the paper proposes a novel flux-switching permanent-magnet spherical motor (FSPMSM). A minimum flux-switching model is modeled, and the tangential force of the rotor-pole tooth in the horizontal direction is analyzed in a one-dimensional space to reduce the cogging torque and the arrangement of the stator and rotor pole tooth is determined. The one-dimensional arrangement is extended to a structural design of a three-dimensional spherical motor and its parameters are determined. According to the high-performance torque zone, the electrifying strategy of a single-coil succession and multiple coil-combination is simulated. The simulation results demonstrate the feasibility of the electrifying strategy and show that FSPMSM achieves a high torque output.

Keywords: Flux-switching permanent magnet spherical motor (FSPMSM); Structural design; Electromagnetic torque; Electrifying strategy.

Zasnova strukture in strategija elektrifikacije sferičnega motorja s trajnim magnetom s preklapljanjem toka

V prispevku predlagamo nov sferični motor s trajnim magnetom s preklapljanjem toka (FSPMSM) za rešitev težav pri strukturah brez jedra v statorski tuljavi sferičnega motorja s trajnimi magneti (PMSM) zaradi nizkega učinkovitega izhodnega navora in nizke gostote moči. Modelirali smo preklapljanja toka in analizirali tangencialno silo rotorja v vodoravni smeri v enodimenzionalnem prostoru. Enodimenzionalno postavitve smo razširili na konstrukcijsko zasnovano tridimenzionalnega sferičnega motorja in določili njegove parametre. Glede na visokozmogljivo navorno območje smo simulirali zaporedje več tuljav. Rezultati simulacije potrjujejo izvedljivost predlagane zasnove in kažejo, da FSPMSM dosega visok izhodni navor.

1 INTRODUCTION

Traditional multi-degree-of-freedom (multi-DOF) actuators are mostly composed of two or more single-degree-of-freedom motors and complex transmission devices [1]. On the one hand, the redundancy in the structure results in a large system volume. On the other hand, complex transmission devices also make a low control accuracy of the system, resulting in a weak system stiffness [2]. The Spherical motor, as a kind of a special motor developed rapidly in recent years, has

many congenital advantages in realizing a multi-DOF motion. Therefore, it has a strong substitution, and has a broad application prospect in the fields of industrial manipulators, robot joints, intelligent motion equipment and so on [3-4].

Various spherical motor structures have been proposed by researchers aiming at a large torque output in order to improve the multi-DOF motion.[5] proposes a new type of the PMSM structure in which two different forms of the stator coil are designed to achieve the spin and tilt motion and the output torque of approx. 0.12 Nm.[4] proposes a PMSM based on the Halbach permanent magnet array.It has a simple rotor permanent-magnet arrangement and optimizes the electromagnetic performance of the PMSM, but the motor output torque is about 0.16 Nm.[7] proposes a stepped PMSM in which the energized stator coil forms an air-gap magnetic field. The rotor poles are permanent magnets, and the poles are arranged in an equally spaced scheme, but the motor output torque is only 0.25 Nm. [8] proposes an innovative two-rotor PMSM and electromagnetic force and electromagnetic torque models of the motor. Unlike the above motors, [9] proposes a reluctance spherical motor where the maximum torque is up to 0.6 Nm due to the fact that the motor driving force is the torque generated by the reluctance. [10] proposes a spherical induction motor

with an axial flux. Compared with the radial flux spherical motor, it reduces the coupling degree between the magnetic fields of different degrees of freedom in the motor and facilitates the decoupling control.

[11] presents to a PMSM which due to its coreless structure, relies only on the hollow coil excitation to interact with the permanent magnet whose shortcoming is a small output torque and low power density. In [12], to further increase the magnetic-field strength, the reluctance spherical motor improves the magnetization effect by introducing a core structure, thus effectively increasing the output torque, but due to its nonlinearity, it also poses certain difficulties for the torque modeling and electromagnetic analysis of the motor.

In recent years, the flux-switching permanent magnet motor (FSPMM), which combines the advantages of the induction and reluctance motor mentioned above, has been widely used in the marine industry and electric drives. Its advantages are a high power, high torque density, coils and permanent magnets are placed on the stator, simple rotor structure without placing any other coils or permanent magnets, and consisting of only a magnetic conductive material, novel structure and good mechanical characteristics [13]. Therefore, in order to increase the output torque of the spherical motor, the paper introduces both the permanent magnet and core structure into the structural design of the motor and proposes FSPMSM. The coil and permanent magnet are placed in the stator structure. The permanent magnet is used as a constant excitation source to provide a magnetic potential. The coil current is used to switch the main flux path and change the position where the air-gap magnetic field appears. The stator and rotor poles of the motor interact electromagnetically to generate tangential forces to drive the rotor motion [14]. The combined structure of the permanent magnets and cores inevitably brings about the problem of a cogging torque. [15] reduces the cogging torque by changing the magnetic-pole parameters and using a new structure with a tooth ring core and multi-stage oblique configuration [16] proposes a new auxiliary slot structure that improves the slot torque amplitude in both degrees of freedom, allowing the motor to obtain a larger deflection angle.

The main contributions of the paper addressing the above issues are:

1. The concept of the flux switching is introduced into a spherical motor for the first time. The minimum flux switching model is established in a one-dimensional space. A tooth groove matching method to suppress the tooth groove torque is proposed. Based on the analysis of a spin motion and tilt motion mechanism, the one-dimensional model is extended to the structure design of the three-dimensional spherical motor. The FSPMM parameters are determined.

2. Based on the analysis of the high torque performance zone in one motion cycle, electrifying strategies are designed and the electromagnetic torque under the two strategies is measured and compared with

the existing high torque reluctance spherical motor. The results demonstrate the FSPMSM feasibility.

The rest of the paper is organized as follows. Section 2, a minimum model of the flux switch is modeled and analyzed. Section 3 introduces a structure design of FSPMSM. Section 4 proposes two driving strategies and comments on the corresponding simulation experiments are carried out to measure the motor torque and prove the FSPMSM feasibility. Section 5 shows conclusions of the performed work.

2 MODELING ANALYSIS OF THE FLUX-SWITCHING MINIMUM MODEL

2.1 Principle

When the rotor rotates, the main flux in the magnetic circuit changes as the relative position between the stator and rotor changes. Figure 1 shows the flux-path diagram for a typical rotor position. The magnetic circuit is composed of stator pole teeth, permanent magnets, air gap and rotor.

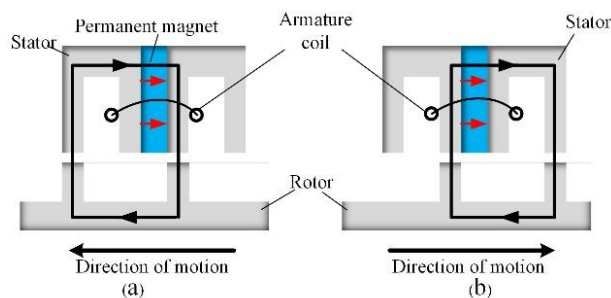


Figure 1. Magnetic-flux path diagram of the rotor in a typical position.

When the rotor is in the position of Figure 1(a), the main flux in the magnetic circuit is closed in the clockwise direction. The magnetic lines of the force passing through the armature coil enter the rotor-pole teeth from the stator pole teeth through the air gap. The rotor-pole teeth are subjected to a leftward tangential force in the horizontal direction. When the rotor is in the position of Figure 1(b), the main flux is still closed in the clockwise direction. The magnetic lines of the force passing through the armature coil enter the stator pole teeth from the rotor pole teeth up through the air gap. The rotor pole teeth are subjected to a tangential force to the right. The force between the stator and rotor teeth during flux-switching is introduced into the design of the spherical motor where the tangential force drives the rotor rotation.

The header and footer on the title page will be set by the editor during final preparation of the manuscript for printing.

2.2 Factors affection flux-switching

Factors affecting flux-switching include the characteristics of the permanent magnet, its size, and the magnitude of the winding coil current.

When no current is applied to the coil, the remanent magnetic strength of the permanent magnet is B_1 and the cross-sectional area in the magnetizing direction is S_1 .

Then the internal magnetic flux of the permanent magnet is:

$$\varphi = \int Bds = B_1 S_1 \quad (1)$$

The effect of the magnetic leakage is ignored. Since the permanent magnet is a constant excitation source, the flux at any position in the magnetic circuit is φ . Each U-shaped magnetic pole tooth contains two magnetic pole teeth. Let the total cross-sectional area of the two magnetic pole teeth be S_3 and the magnetic induction intensity be B_3 . Then:

$$\varphi = B_1 S_1 = B_3 S_3 \quad (2)$$

Bringing the remanent magnetic strength of the permanent magnet and the critical saturation magnetic induction strength of the stator pole teeth into the above equation, we have:

$$1.2T \cdot S_1 = 1.8T \cdot S_3 \quad (3)$$

$$S_1 : S_3 = 3 : 2 \quad (4)$$

Considering that the U-shaped magnetic pole tooth contains two magnetic pole teeth, then:

$$S_3 = 2S_2 \quad (5)$$

Finally we get:

$$S_2 : S_1 = 1 : 3 \quad (6)$$

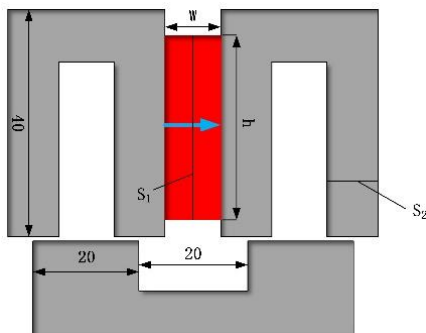


Figure 2. Effect of the permanent-magnet parameters on the main magnetic-circuit flux.

In Figure 2, W is the variation of the thickness of the permanent magnet, h is the variation of the height of the permanent magnet, S_1 is the cross-section of the magnetization direction of the permanent magnet, and S_2 is the cross section of the magnetic pole tooth. By changing the thickness of permanent magnet W , integral

Φ_1 of magnetic induction intensity B_1 in the permanent magnet on the S_1 surface and integral Φ_2 of the magnetic induction intensity B_2 in the U-shaped pole tooth on the S_2 surface are calculated. The thickness of permanent magnet W varies from 5mm to 15mm with a uniform interval of 1mm.

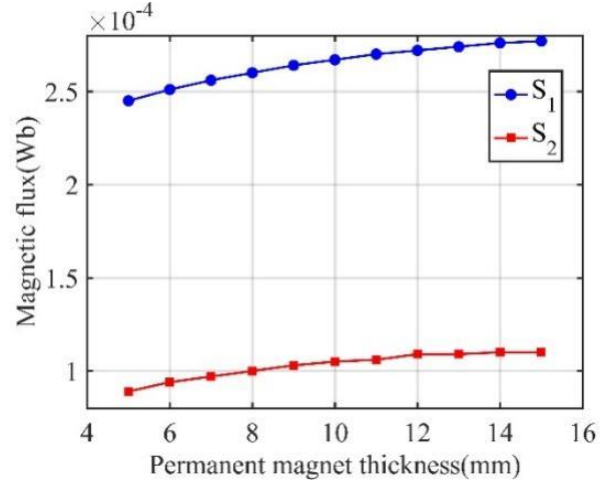


Figure 3. Fluxes in S_1 and S_2 for different permanent magnets thicknesses.

As seen in Figure 3, when the thickness of the permanent magnet increases, the flux change on the surface increases slowly and in a small range, and the rising trend of the curve gradually becomes slower. The permanent magnet of a certain thickness for the magnetic induction intensity and the flux change in the magnetic circuit is not obvious. Considering the flux change curve and the symmetry of the model structure, the thickness of the permanent magnet is 10mm at the center position and the width of the stator U-shaped pole teeth is the same, which is convenient for the symmetrical and uniform arrangement of the structure.

The remanent magnetic strength of the permanent magnet is certain, and its internal magnetic flux is equal to the product of the area vector and the magnetic induction intensity vector. The change in the cross-sectional area of the magnetizing direction of the permanent magnet directly leads to a change in the magnetic flux in the main magnetic circuit. As shown in Figure 4, the thickness of the permanent magnet is unchanged, the width is 10mm and the parameter is set to calculate the magnitude of the horizontal tangential force on the rotor U-shaped pole teeth after applying the current to the coil at the heights of 10mm, 20mm, 25mm, 30mm, 35mm, and 40mm, respectively.

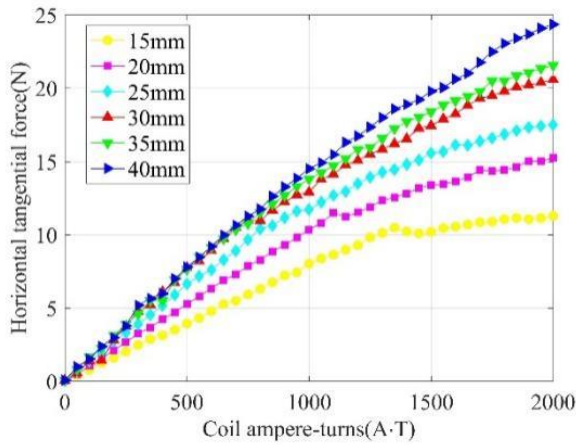


Figure 4. Tangential force on the rotor pole teeth for different permanent magnet heights.

Setting the coil current ampere turns range to 0-2000A·T(ampere-turn).Figure 4 shows the tangential force curves for the permanent magnet heights h of 30mm, 35mm and 40mm, and the three curves almost coincide when the number of the turns does not exceed 1000A·T. At smaller current turns (within 1000A·T), when the permanent magnet height is greater than 30mm, the increase in the area is small because of the change in the horizontal tangential force. Therefore, the height of the permanent magnet is 30mm. Combined with the above equation, the simulation parameters are selected in accordance with the proportional relationship, which provides the basis for the further design of the motor structure.

3 STRUCTURAL DESIGN OF FSPMSM

3.1 Cogging torque for the flux-switching model

Due to the presence of the permanent magnets, the excitation flux generated by the permanent magnets inevitably generates the cogging torque. Its presence causes vibration and noise in the motor, torque pulsation and affects the smooth operation of the motor. The cogging torque is actually the negative derivative of magnetic-field energy storage W with respect to the deflection angle when the coil is not energized:

$$T_{cog} = -\frac{\partial W}{\partial \alpha} \quad (7)$$

Where is the relative position angle between the upper pole pair and the rotor pole tooth.

In the analysis, the following assumptions are made:

- (1) The magnetic permeability of the pole tooth core is infinite;
- (2) Neglecting the leakage phenomenon and edge effect in the model, the air-gap magnetic density is assumed to be 0 at the position where the stator and rotor pole teeth do not overlap.

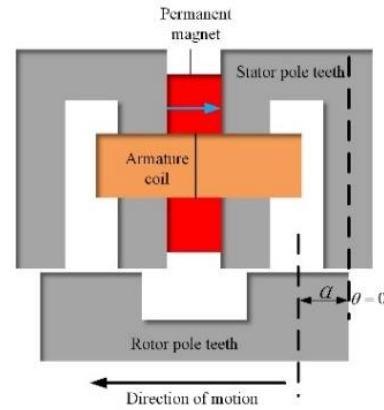


Figure 5. Schematic diagram of the relative positions of the stator pole pair and the rotor pole teeth.

Based on the above assumptions, the magnetic field energy in the flux-switching model is approximately equal to the energy stored in the air gap and permanent magnets. The permanent magnet and the air gap between the stator and rotor both have magnetic fields in the model, and the permanent magnet can be approximated it no change in the energy due to its placement in the stator structure, i.e., only the change in the magnetic-field storage in the air gap leading to the generation of a slot torque is considered. Thus the expression is transformed to:

$$T_{cog} = -\frac{\partial W}{\partial \alpha} = -\frac{\partial (W_{gap} + W_{pm})}{\partial \alpha} \approx -\frac{\partial W_{gap}}{\partial \alpha} \quad (8)$$

The magnetic-field energy in the air gap can be expressed as:

$$\begin{aligned} W_{gap} &= \frac{1}{2\mu_0} \int_v B_\delta^2(\theta) dV \\ &= \frac{1}{2\mu_0} \int_v B_r^2(\theta) \left(\frac{h_m(\theta)}{h_m(\theta) + \delta(\theta, \alpha)} \right)^2 dV \end{aligned} \quad (9)$$

In equation 1, $B_\delta(\theta)$ is the magnetic field of the air gap between the stator and rotor; $B_r(\theta)$ is the remanent magnetization of the permanent magnet; $\delta(\theta, \alpha)$ is the effective air gap length; $h_m(\theta)$ is the distribution of the magnetization length of the permanent magnet along the circumferential direction; The $\theta = 0$ position is set on the centerline of the rotor pole teeth; Stator-rotor deflection angle α is the angle between the centerline of the rotor teeth and the centerline of the magnetic pole pair.

From equation 3, the Fourier expansion expressions for $B_r^2(\theta)$ and $\left(\frac{h_m(\theta)}{h_m(\theta) + \delta(\theta, \alpha)} \right)^2$ are obtained, which leads to the expression for the cogging torque.

The period of change of $B_r^2(\theta)$ is one stator tooth pitch. The fourier expansion of $B_r^2(\theta)$ in one cycle of a change:

$$B_r^2(\theta) = B_{r,0} + \sum_{n=1}^{\infty} B_{r,n} \cos N_s n\theta \quad (10)$$

$$B_{r,0} = \frac{\beta_s B_r^2}{\tau_s} ; B_{r,n} = \frac{2}{n\pi} B_r^2 \sin \frac{n\beta_s}{\tau_s} \pi ; N_s \text{ is the}$$

number of the stator poles; B_r is the remanent magnetic density of the permanent magnet; β_s is the width of the magnetic pole tooth above the model expressed in angular radians; τ_s is the angular radian indicating the pole distance between the two magnetic pole teeth above.

Without considering the edge effect and leakage phenomenon, the length of the air gap between the rotor pole teeth and the stator pole teeth is δ . The length of the air gap corresponding to the slot of the magnetic pole is considered to be infinite. The Fourier expansion

of $\left(\frac{h_m(\theta)}{h_m(\theta) + \delta(\theta, \alpha)} \right)^2$ is:

$$\left(\frac{h_m(\theta)}{h_m(\theta) + \delta(\theta, \alpha)} \right)^2 = G_0 + \sum_{m=1}^{\infty} G_m \cos N_r \theta \quad (11)$$

Where N_r is the number of the rotor tooth poles. When changing the relative positions of the stator-pole teeth and rotor-pole teeth in the model, it is equivalent to the increase in the initial phase of the above equation.

The Fourier expansion of $\left(\frac{h_m(\theta)}{h_m(\theta) + \delta(\theta, \alpha)} \right)^2$ then

can be expressed as follows:

$$\left(\frac{h_m(\theta)}{h_m(\theta) + \delta(\theta, \alpha)} \right)^2 = G_0 + \sum_{m=1}^{\infty} G_m \cos N_r(\theta + \alpha) \quad (12)$$

$$G_0 = \frac{\beta_r G_s}{\tau_r} , G_m = \frac{2}{m\pi} G_s \sin \frac{m\beta_r}{\tau_r} \pi , N_r \text{ is the}$$

number of the rotor-pole tooth stages; β_r is the width of the rotor-pole teeth expressed in angular radians; τ_r is the pole pitch of the stator pole expressed in angular

$$\text{radians; } G_s = \left(\frac{h_m}{h_m + \delta} \right)^2 .$$

Bring Eq.9~Eq.12 into Eq.8. Use the characteristics of the trigonometric functions integrated in $[0 \sim 2\pi]$:

$$\begin{cases} \int_0^{2\pi} \cos m\theta \cos n\theta d\theta = 0 & m, n = 1, 2, 3 \dots m \neq n \\ \int_0^{2\pi} \cos^2 m\theta d\theta = 0 & m = 1, 2, 3 \dots \end{cases} \quad (13)$$

Then the expression for the cogging torque of the model is:

$$T_{cog}(\alpha) = \frac{\pi N_r l_{Fe}}{4\mu_0} (R_2^2 - R_1^2) \sum_{m=1}^{\infty} n G_m B_r \frac{n N_r}{N_s} \sin n N_r \alpha \quad (14)$$

In Eq.14, l_{Fe} is the axial length of the magnetic pole tooth, R_1 and R_2 are the radius of the rotor pole tooth and the radius of the stator pole tooth, respectively.

Based on the above analysis, the analytical model of the cogging torque is set up. By studying the formula and changing some parameters, the method of reducing the cogging torque is obtained which also provides a certain theoretical basis.

3.2 One-dimensional spatial pole tooth arrangement to reduce the tooth slot torque

To analyse and describe of the tooth slot torque, the arrangement is first studied in a one-dimensional space and then extended to a three-dimensional space arrangement. The arrangement of the stator-pole pairs in a one-dimensional space is shown in Figure 6:

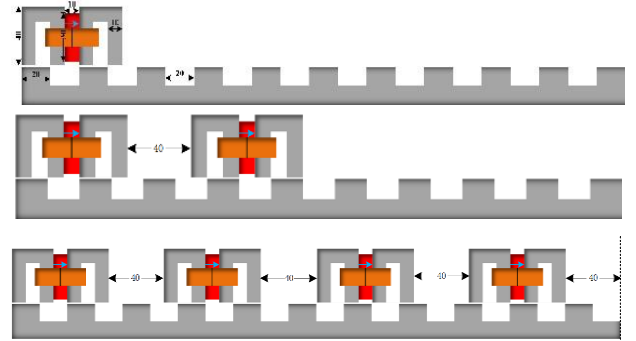


Figure 6. Arrangement of the stator-pole pairs in a one-dimensional space.

The model in Figure 6 first places a stator pole pair, and the parameters of the stator U-shaped pole teeth and permanent magnets are consistent with the flux-switching minimum model in Section 2. Next, in the case of two-pole pairs as well as four-pole pairs, the arrangement is studied in order to reduce the tangential force causing the tooth slot torque through the interplay between two and two.

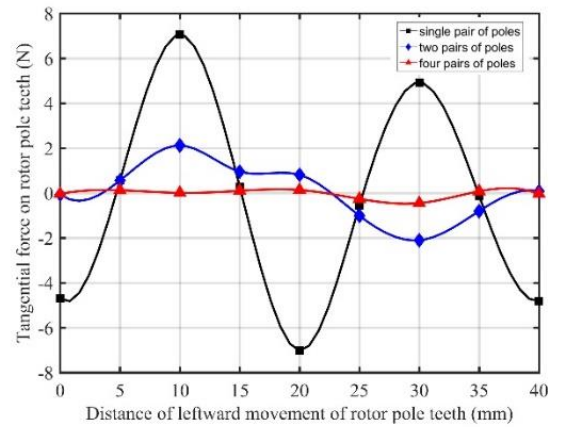


Figure 7. Fitted curves of the magnetic pole pairs in a range of the tooth pitch tangential forces.

As seen in Figure 7, the peak tangential component is 7.8 N for a single-pole pair and only 2.1 N for a two-pole pairs. The arrangement effectively offsets the horizontal tangential component of the force between the stator and rotor teeth and it reduces the torque of the tooth groove. The tangential component of the force in the four-pole pairs arrangement pulsates around 0. Its value is much smaller than 2.1 N in the two-pole pair, which is more effective in suppressing the tangential component. Combined with the actual size of the spherical motor, the current arrangement of four stator pole pairs and 11 rotor pole teeth is more suitable, so the arrangement in the one-dimensional space is determined as this arrangement.

3.3 Stator-rotor structure of FSPMSM

The spin and tilt motion are the two basic types of the motion for the three-dimensional space motion of the spherical motors. Firstly, the spin motion mechanism of FSPMSM is analyzed as shown in Figure 8:

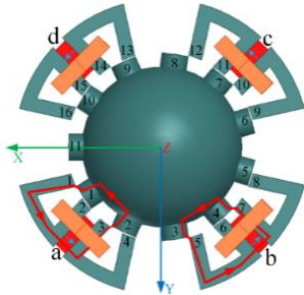


Figure 8. Spin motion mechanism.

The mechanism of the rotor spin motion is illustrated according to the stator arrangement in Figure 8. The stator four-pole pairs are arranged in the XY plane and 11 rotor pole teeth are arranged along the circumference of the rotor, and each parameter is consistent with the structure in Figure 6.

Taking the a-phase pole pair as an example, the a-phase is passed into the reverse direction current which generates an air gap magnetic field in the stator one- and three-pole teeth. The one- and three-pole teeth together with their nearest rotor one- and two-pole teeth form a magnetic flux circuit, and the magnetic lines of the force are closed in the counter clockwise direction. The clockwise tangential electromagnetic force on the rotor teeth around the Z-axis drives the rotor in a clockwise spin. (The current direction which is the same as the magnetization direction of the permanent magnet is specified as a forward current, and the opposite is a reverse current.)

Figure 9 shows the same mechanism as for the spin motion, the tilt direction using a similar arrangement with the spin motion when the rotor attains the characteristics of the tilt motion, and the arrangement of the stator and rotor magnetic pole teeth:

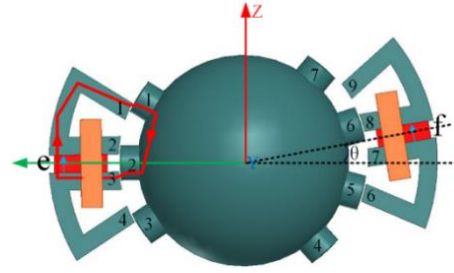


Figure 9. Tilt motion mechanism.

The tilt motion is defined as the rotor clockwise rotation or the counter clockwise rotation around the Y-axis. In Figure 9, three rotor pole teeth are evenly spaced on the left side and four on the right side, with 32.72° between each rotor pole tooth, 1, 2, 3 rotor pole teeth and 4, 5, 6, 7 rotor-pole teeth are arranged along the circumference of the XZ plane. Because each rotor pole tooth is located in the latitude line, 11 pole teeth need to be arranged along the circumference, when the dimension is higher than 4, 7 pole teeth, there will be an insufficient space between the pole teeth cross each other. So due to its own structure, the pole teeth cannot be arranged in a higher latitude considering the maximum range of the motion in accordance with this arrangement.

3.4 Layout scheme of the stator-rotor structure

Based on the arrangement scheme of the spin and tilt motion, the motor structure scheme in Figure 10 is obtained by combining the stator and rotor pole teeth.

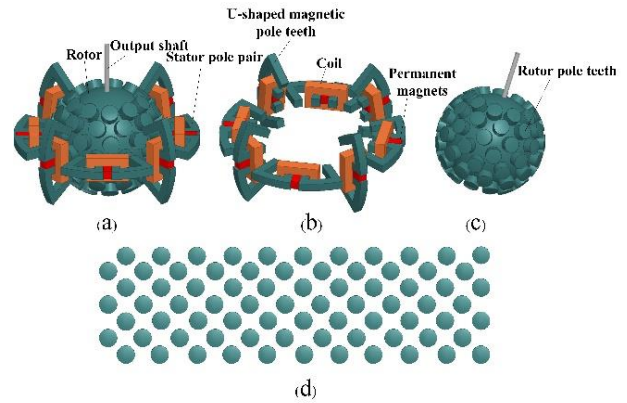


Figure 10. Schematic diagram of the motor stator and rotor structure.

FSPMSM is divided into the stator and rotor body. As shown in figure 10(b), the stator body consists of eight magnetic pole pairs of which four equally spaced in the equatorial plane complete the spin motion at an interval of 90° and the remaining four vertically spaced along the meridian in the circumference complete the tilt motion. The rotor teeth are placed on the hollow permeable sphere, and the 11 pole teeth are evenly distributed along the equatorial plane, each two pole teeth are separated by 32.72° . There are seven layers

which are separated by 16.36° . The upper and lower layers are arranged alternatively. The arrangement is shown in a planar expansion diagram in Figure 10(d).

3.5 Structure parameters of FSPMSM

Based on the simulation analysis of the parameters affecting the performance of the motor, the impact of the rotor tooth radius, air gap width and coil current size on the electromagnetic torque and slot torque of the motor are analyzed and the structural parameters of the motor are determined by the comprehensive simulation results shown in Table 1:

Parameters	Value
Stator outer diameter / mm	110
Stator inner diameter / mm	70
Stator pole tooth width / mm	10
Stator pole tooth height / mm	30
Thickness of permanent magnets / mm	10
Length of permanent magnets / mm	30
Width of permanent magnets / mm	10
Rotor outer diameter / mm	69
Rotor pole tooth height / mm	10
Rotor pole tooth radius / mm	10
Air gap width / mm	1
Number of turns of coils	1000

4 ELECTROMAGNETIC TORQUE OF FSPMSM

The three-degree-of-freedom motion of the rotor can be divided into three basic rotations: spin, pitch and yaw. The spin motion of the rotor rotation around the Z-axis and the pitch and yaw can be summarized as a tilt motion which is the rotor rotation around the X- or Y-axis.

Since the mechanism of the rotor spin motion is the same as that of the tilt motion, only the rotor spin motion and measure account of electromagnetic torque will be discussed.

4.1 Moment-angle characterization

In order to operate the motor always in the high-torque performance region, the moment angle characteristics under one motion cycle are analysed. All the discussed coil-current revolves are set to 1000 amp turns.

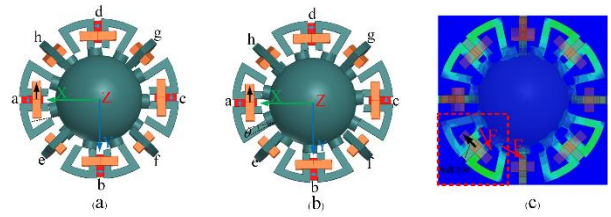


Figure 11. Schematic diagram of the motor single coil energized to drive the rotor rotation.

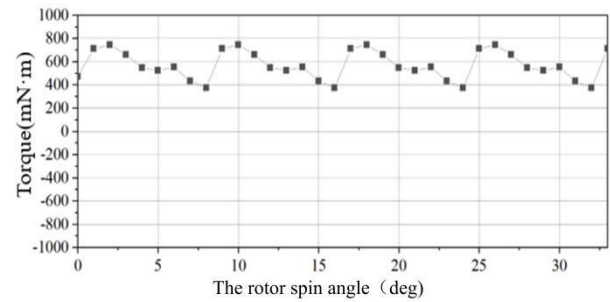


Figure 12. A-phase coil energized rotor spin-motion moment characteristic angular distribution.

When the motor rotor is in the position shown in Figure 11(a), the a-phase coil is passed into the forward current (the current is counter clockwise in the positive direction and clockwise in the opposite direction when viewed from the outside of the motor), the equatorial surface magnetic-field distribution cloud of the motor is shown in Figure 11(c), and the rotor pole teeth are subjected to a positive electromagnetic torque of the Z-axis under the action of the air-gap magnetic field below the stator pole teeth, and can be turned to the position shown in Figure 11(b), and the angle is turned by θ (i.e. about 8°). When the rotation exceeds 8° , the electromagnetic torque decreases to a lower value as shown in Figure 12 of the a-phase coil electromagnetic torque distribution. This happens when the stator teeth are completely above the rotor pole teeth and the tangential force on the rotor teeth at this point is much lower. When the rotor is about to enter the low-torque region of this phase coil, switching to the next phase energizes the rotor so that the rotor remains in the higher torque region.

4.2 Single-coil electrifying strategy

An electrifying strategy is used to energize the single coil to complete the continuous rotation of the motor rotor.

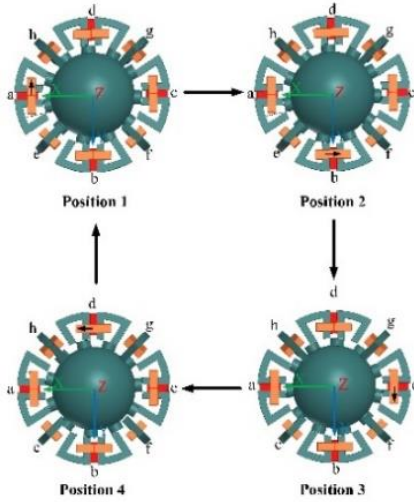


Figure 13. Single coil continuously energized to drive the rotor continuous spin rotation scheme.

The phase change is illustrated in relation to Figure 11, taking position 1 and position 2 as examples. When the motor rotor is in position 1, the a-phase is energized with a positive current and the rotor is rotated by the electromagnetic force in the positive direction around the Z-axis. When the rotor rotates to position 2 and the a-phase continues to be energized, the rotor enters the low torque region and the effective electromagnetic torque generated by the current is low. Take the way to switch to the b-phase coil energized, in position 2 of the b-phase coil energized into the reverse current, the rotor in the b-phase coil of the high torque region to continue to move to position 3, and so on, to c-phase, d-phase, in re-return to a-phase, continue the cycle, completes the continuous spin rotation.

Table 2. Spin-motion single-coil electrified mode current direction

Coils	direction			
	a	b	c	d
Position 1	+			
Position 2		-		
Position 3			+	
Position 4				-

Table 2 shows the direction of the coil currents when the rotor is in different positions. The corresponding torque when the rotor is in different positions is shown in Figure 14.

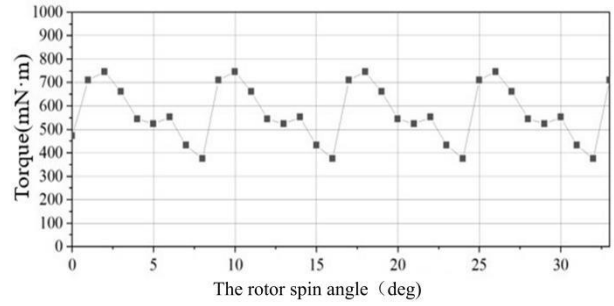


Figure 14. Schematic diagram of the corresponding torque when the rotor spins through different angles in a single-coil electrified mode.

The above figure shows the electromagnetic torque distribution of the rotor rotating one tooth pitch range. The peak torque is about 750mNm. According to the above electrifying strategy, continue to cycle the electrified of the a,b,c,d phase coils until it completes the continuous rotation of the rotor.

4.3 Multi-coils electrifying strategy

To achieve the maximum torque output for the motor spin motion, multiple coils are simultaneously connected to the current so that the electromagnetic torque generated by each coil is in the same direction as the required torque and the torque is superimposed to achieve a maximum electromagnetic torque output. The number of the Ampere turns of each coil is set to 1000A·T. When at the current position shown in Figure 15, the phase a coil is connected to a forward current, the phase b coil is connected to a forward current, the phase c coil is connected to a reverse current, and the phase d coil is connected to a reverse current, all four coils produce a positive Z-axis torque.

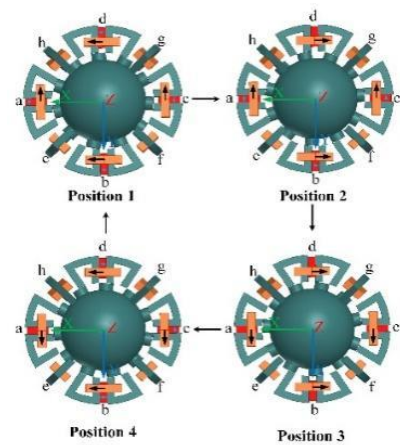


Figure 15. Multi-coil energized rotor spin schematic.

Table 3 shows the direction of the coil current at different positions.

Table 3. Spin motion multi-coils electrified mode current direction

Coils	a	b	c	d
Position 1	+	+	-	-
Position 2	+	-	-	+
Position 3	-	-	+	+
Position 4	-	+	+	-

Figure 16 shows different angles at a spin motion :

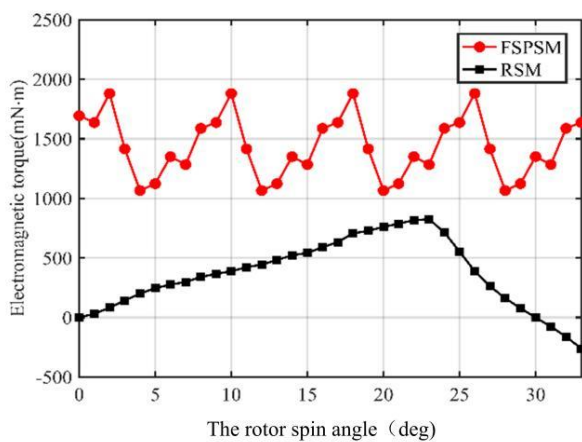


Figure 16. Torque at different angles.

Figure 16 shows that the electromagnetic torque generated at a spin motion with multiple electrified coils is higher. The peak torque is about 1.9 N·m. Compared to the reluctance spherical motor, the output electromagnetic torque of the flux-switching spherical motor is increased by about 130%.

5 CONCLUSION

The paper presents the design of a multi-freedom FSPMSM structure and describes the basic principle of flux switching and the factors affecting it. By determining the motor layout in a one-dimensional space, a minimum-flux switching model is established to reduce the slot torque and increase the output electromagnetic torque. Two electrifying strategies are designed and based on the simulation results, the FSPMSM feasibility is verified. In future, FSPMSM will be applied in the field of the robot joint wrist, multi-DOF robot arm for the space station, bionic eye, etc.

ACKNOWLEDGEMENT

The work was financially supported by the Key Projects of the Regional Innovation Joint Fund of the National

Natural Science Foundation of China(U23A20647), the National Natural Science Foundation of China (No. 51637001, No.51307001), the Natural Science Foundation of Anhui Province (2008085ME156).

REFERENCES

- [1] Y. Wen, Z. Liu, Q. Wang *et al.*, "Continuous non-singular terminal sliding-mode control of permanent magnet spherical actuator for trajectory tracking based on a modified nonlinear disturbance observer," *IET Electr. Power Appl.*, vol. 16, no. 8, pp. 896-911, 2022.
- [2] Li, X., J. Liu, W. Chen, and S. Bai. "Integrated design, modeling and analysis of a novel spherical motion generator driven by electromagnetic principle," *Robot. Auton. Syst.*, Vol. 106, 2018, pp. 69-81.
- [3] Ju L, Tao W, Wang Q, *et al.* "Nonlinear modeling analysis of a reluctance spherical motor based on torque-angle characteristics," *Int. J. Appl. Electromagn. Mech.*, 2019, 62(1):1-17.
- [4] Chai, F., L. Gan, and L. Chen. "A novel tiered type permanent magnet spherical motor and its rotor orientation measurement principle," *IEEE Access*, Vol. 8, 2020, pp. 15303-15312.
- [5] PARK H J, CHO S Y, AHN H W, *et al.* "A Study of Advanced Spherical Motor for Improvement of Multi-DOF Motion," *J. Electr. Eng. Technol.*, 2012, 7(6): 926-31.
- [6] XIA C, GUO C, SHI T. "A Neural-Network-Identifier and Fuzzy-Controller-Based Algorithm for Dynamic Decoupling Control of Permanent-Magnet Spherical Motor," *IEEE Trans. Ind. Electron.*, 2010, 57(8): 2868-78.
- [7] Wen Y, Li G, Wang Q, *et al.* "Investigation on the measurement method for output torque of a spherical motor," *Appl. Sci.-Basel*, 2020, 10(7): 2510.
- [8] Yan L, Chen I M, Lim C K, *et al.* "Modeling and iron-effect analysis on magnetic field and torque output of electromagnetic spherical actuators with iron stator," *IEEE-ASME Trans. Mechatron*, 2011, 17(6): 1080-1087.
- [9] Shi M, Wang Q, Li G, *et al.* "A New Adaptive Analytical Model for the Spherical Reluctance Motor Based on Hybrid Trigonometric Function-Power Function," *IEEE Trans. Ind. Electron*, 2022.
- [10] Huai Z, Zhang M, Zhu Y, *et al.* "A Novel Electrodynamic Reaction Sphere Prototype for Spacecraft Attitude Control," *IEEE Trans. Ind. Electron*, 2020, 67(5): 3879-3890.
- [11] Sulaiman E, Ahmad M Z, Kosaka T, *et al.* "Design Optimization Studies on High Torque and High Power Density Hybrid Excitation Flux Switching Motor for HEV," *Procedia Engineering*, 2013, 53(7):312-322.
- [12] R. Thike, and P. Pillay, "Mathematical Model of an Interior PMSM With Aligned Magnet and Reluctance Torques," *IEEE Trans. Transp. Electrification*, vol. 6, no. 2, pp. 647-658, 2020.
- [13] Y. Shi, L. Jian, J. Wei *et al.*, "A New Perspective on the Operating Principle of Flux-Switching Permanent-Magnet Machines," *IEEE Trans. Ind. Electron*, vol. 63, no. 3, pp. 1425-1437, 2016.
- [14] R. Cao, and M. Lu, "Investigation of High Temperature Superconducting Linear Flux-Switching Motors With Different Secondary Structures," *IEEE Trans. Appl. Supercond*, vol. 30, no. 4, pp. 1-5, 2020.
- [15] L. Mo, T. Zhang, and Q. Lu, "Design and Analysis of an Outer-Rotor-Permanent-Magnet Flux-Switching Machine for Electric Vehicle Applications," *IEEE Trans. Appl. Supercond*, vol. 29, no. 2, pp. 1-5, 2019.
- [16] Z. Li, X. Yu, X. Wang *et al.*, "Optimization and Analysis of Cogging Torque of Permanent Magnet Spherical Motor," *IEEE Trans. Appl. Supercond*, vol. 31, no. 8, pp. 1-5, 2021.

Xiwen Guo received his Ph.D. degree in electrical engineering from the Hefei University of Technology, China, in 2012. Currently, he is an associate professor at the School of Electrical Engineering and Automation at the Anhui University of China. His research interest is in special motors and their control, power electronics and electric drives, intelligent control, and motor-pump modelling.

Zhibo Liu graduated from the School of Electrical Engineering and Automation, Civil Aviation University of China in 2022. He is currently working towards his M.S. degree at the School of Electrical Engineering and Automation of the Anhui University of China. His research interest is in special motor design.

Zhaowei Fang graduated from Huainan Normal University, School of mechanical and electrical engineering in Huainan, China, in 2019. He is currently working towards his M.Sc. degree at the School of Electrical Engineering and Automation of the Anhui University of China. His research interest is in special motor design.

Rui Zhou received his Ph.D. degree from the Anhui University, Hefei, China. His research interest is in electrical machines design.

Qunjing Wang received his Ph.D. degree from the University of Science and Technology of China, Hefei, China, in 2001. Currently, he is a professor at the School of Electrical Engineering and Automation at the Anhui University of China. His research interest is in electrical machines, motor drives and novel electric drive systems.

Ronglin Zhang graduated from the Architecture University of Anhui, College of mechanical and electrical engineering in Hefei, China, in 2019. He received his M.Sc. degree from the Anhui University in 2022. He is currently working with State Grid Lu'an Electric Power Supply Company.